PET/MR Imaging and Optical Imaging of Metastatic Rhabdomyosarcoma in Mice

Sorin Armeanu-Ebinger*[1], Christoph M. Griessinger*[2], Delia Herrmann[1], Jörg Fuchs[1], Manfred Kneilling[2,3], Bernd J. Pichler[2], and Guido Seitz[1]

[1]Department of Pediatric Surgery and Urology, University Children's Hospital, Eberhard Karls University Tübingen, Tübingen, Germany; [2]Department of Preclinical Imaging and Radiopharmacy, Werner Siemens Imaging Center, Eberhard Karls University Tübingen, Tübingen, Germany; and [3]Department of Dermatology, Eberhard Karls University Tübingen, Tübingen, Germany

The combination of PET and MR imaging synergizes molecular and morphologic information, allowing better diagnosis in cancer patients. The diagnosis of tumor recurrence in rhabdomyosarcoma is extremely challenging and could be improved with PET/MR imaging. The aim of this study was to validate PET/MR imaging in a disseminated rhabdomyosarcoma mouse model. **Methods:** One million alveolar (Rh30) and embryonal (RD) rhabdomyosarcoma cells with stably transfected mCherry and Gaussia luciferase were injected intraperitoneally into NOD/LtSz-scid-IL2Rynull mice. Nine animals were treated with vincristine (0.75 μg/g/d). Tumor growth was monitored on the basis of serum luciferase activity, optical imaging (OI) of the fluorescent protein mCherry, and sequential PET/MR imaging with 3′-deoxy-3′-^{18}F-fluorothymidine (^{18}F-FLT) and ^{18}F-FDG. Immunohistochemical Ki-67 and glucose transporter 1 analysis was used to evaluate tumor cell density and proliferative and metabolic activity. **Results:** The injection of rhabdomyosarcoma cells led to intraperitoneal tumor growth in 34 of 37 mice (Rh30) and 4 of 9 animals (RD). OI revealed inconsistent results for tumors located near the liver. The detection of tumors in the peritoneal cavity was exclusively possible with sequential PET/MR imaging. PET studies with ^{18}F-FLT MR imaging were more reliable than ^{18}F-FDG comparing the tracer uptake and correlation with tumor weight. Treatment with vincristine led to reduced tumor growth, which was efficiently detected with ^{18}F-FDG PET and MR imaging. Total tumor burden as estimated by PET/MR imaging correlated with the serum luciferase activity. **Conclusion:** We established a unique model of metastatic rhabdomyosarcoma with a high frequency of tumor occurrence and easy monitoring of the tumor growth based on reporter gene expression. The accurate detection of rhabdomyosarcoma requires high soft-tissue contrast provided by the MR imaging and high tracer uptake for PET, which was achieved with ^{18}F-FLT as the tracer before and ^{18}F-FDG after treatment with vincristine. PET/MR imaging allows improved diagnosis of experimental rhabdomyosarcoma and therefore might influence clinical therapeutic decisions in the future.

Key Words: rhabdomyosarcoma; metastasis; xenograft; luciferase; mCherry; ^{18}F-FDG; ^{18}F-FLT; PET/MRI; combination

J Nucl Med 2014; 55:1545–1551
DOI: 10.2967/jnumed.114.138578

Received Feb. 5, 2014; revision accepted May 6, 2014.
For correspondence or reprints contact: Sorin Armeanu-Ebinger, Department of Pediatric Surgery and Urology, University Children's Hospital, Hoppe Seyler Strasse 3, 72076 Tübingen, Germany.
E-mail: armeanu@uni-tuebingen.de
*Contributed equally to this work.
Published online Jun. 24, 2014.

Soft-tissue sarcomas originate from mesenchymal tissues and represent 15% of all solid pediatric tumors. Rhabdomyosarcomas are the most common subtype (*1,2*). Risk factors that predict outcome are size and invasiveness, primary site, complete surgical removal, patient age, histology, and metastatic spread (*1,2*). Noninvasive imaging can identify several of these risk factors and provides essential information for staging and therapy monitoring.

MR imaging provides detailed anatomic information with high soft-tissue contrast and is currently the state-of-the-art imaging modality for the detection of rhabdomyosarcoma (*3*). Molecular imaging with PET reveals the metabolic activity of tumors and improves the detectability of primary lesions and metastases by yielding high detection sensitivity (*4*). In combination with CT, PET was proposed as a predictor of outcomes and to refine risk-adapted therapy (*5,6*). PET/CT has a low acceptance in the clinical routine in children because the radiation exposure is often considered too high (*7*) and can reach a mean effective dose of 10 mSv (*8*). The PET/CT method also has limitations in the detection of smaller lesions, in well-differentiated tumors, or in cases of low metabolic rates (*9*). A major diagnostic problem of PET/CT is the discrimination between remnant scar tissue and tumor relapse, which is usually revealed on MR imaging (*9*). Therefore, PET/MR imaging, a relatively new multimodality imaging system, which is used in preclinical research and has recently entered the clinic, may further improve rhabdomyosarcoma imaging and offer complementary information for the assessment of suggestive structures (*10–15*). Different PET tracers, such as the glucose analog ^{18}F-FDG, ^{18}F-fluoromethylcholine, or hypoxia markers, have already been tested in subcutaneous rodent rhabdomyosarcoma models, demonstrating their feasibility in the detection and monitoring of rhabdomyosarcoma during therapy (*16–20*). 3′-deoxy-3′-^{18}F-fluorothymidine (^{18}F-FLT) PET imaging has been applied in different sarcomas but not in rhabdomyosarcoma (*21,22*).

Questions regarding tumor biology, tumor immunology, and immunotherapy in rhabdomyosarcoma are challenging and require advanced animal models to be adequately studied (*23*). Xenograft models of human rhabdomyosarcoma normally develop subcutaneous tumors and are of limited use in the investigation of metastatic disease (*24*). To date, a spontaneous model of rhabdomyosarcoma in mice has been developed (*25*), but there are no reproducible disseminated human rhabdomyosarcoma models.

The aim of our study was to establish an animal model of disseminated human rhabdomyosarcoma and to evaluate ^{18}F-FDG, ^{18}F-FLT, and ^{11}C-choline PET tracers using sequential PET/MR or PET imaging as the diagnostic approach in disseminated rhabdomyosarcoma. The 3 tracers were chosen on the basis of the existing literature on rhabdomyosarcoma and other sarcomas and on the fact that

they are approved in several institutions for clinical trials in patients, which enables translational studies.

MATERIALS AND METHODS

Cells and Animal Model

10^6 RD or Rh30 tumor cells expressing Gaussia luciferase (GLuc) and mCherry were injected intraperitoneally into 8-wk-old NOD/LtSz-scid IL2Rγnull mice (NSG, Jackson Laboratories) (supplemental data; supplemental materials are available at http://jnm.snmjournals.org). Nine mice were additionally treated 21 d after xenotransplantation (Rh30) with 0.75 μg of vincristine per kg of body weight at 2 consecutive days. The experimental design is given in Table 1. All studies were approved by the responsible animal welfare authority (K 02/10). Serum samples were obtained 14 and 21 d after xenotransplantation by drawing retro bulbar blood. GLuc activity as relative light units per second was measured in the serum (*26*). Optical imaging (OI) and sequential PET/MR imaging were performed 3 and 4 wk after injection.

OI

In vivo OI fluorescence and bioluminescence signals were detected with the macroscopic imaging system Aequoria, including the dual-mode cooled charge-coupled device Camera OrcaII-BT1024 and the Hokawo 2.1 software (Hamamatsu Photonics) (supplemental data). Tumors with a fluorescence area lower than 1 mm^2 in OI were confirmed at the higher magnification (200×) in the fluorescence microscopy.

Sequential PET/MR Imaging

The radioactive isotopes for the PET tracers ^{18}F-FDG, ^{18}F-FLT, and ^{11}C-choline, for the detection of intraperitoneal rhabdomyosarcoma tumors by sequential PET/MR imaging, were produced with a 16-MeV PETtrace Cyclotron (GE Healthcare) at the Department of Preclinical Imaging and Radiopharmacy, Tübingen, Germany (supplemental data).

For PET tracer evaluation in the preclinical rhabdomyosarcoma model, sequential PET/MR imaging was performed with the tracers ^{18}F-FDG and ^{18}F-FLT 3–4 wk after xenotransplantation. ^{18}F-FDG PET/MR imaging was performed in the morning and ^{18}F-FLT PET/MR imaging in the afternoon of the same experimental day. However, because of logistic constraints, ^{11}C-choline PET scans were obtained 2 d later without MR imaging in the same animals.

For the evaluation of the effects of cytotoxic agents by PET/MR imaging, vincristine was administered on 2 consecutive days 3 wk after xenotransplantation as described above. For therapy monitoring, baseline PET/MR imaging with ^{18}F-FDG and ^{18}F-FLT was performed before vincristine treatment and 2 and 4 wk after treatment.

In vivo PET scans were acquired with a small-animal Inveon microPET scanner (Siemens Medical Solutions) (Table 2) (supplemental data). After the PET scans, animals were transferred on the mouse bed to a 7-T small-animal MR scanner (ClinScan; Bruker Biospin MR Imaging) equipped with a quadrature mouse whole-body coil (diameter, 35 mm). Reconstructed PET images were corrected for radioactive decay and normalized to the injected activity. According to our standard PET protocol for mice, attenuation correction was not applied. The PET images were coregistered with the corresponding MR scans using analysis software (Inveon Research Workplace; Siemens Medical Solutions). Volumes of interest were drawn in the PET images on the intraperitoneal rhabdomyosarcoma tumors based on the anatomic information of the MR image. For data analysis, the percentage injected dose per centimeter cubed (%ID/cm^3) was calculated.

Biodistribution

Eight Rh30-bearing experimental mice were injected with ^{18}F-FDG ($n = 4$) or ^{18}F-FLT ($n = 4$) 3 wk after the intraperitoneal tumor inoculation, sacrificed after the tracer uptake time (Table 2), and dissected. Explanted tumors were evaluated by ex vivo fluorescence OI scans and weighed, and the activity in the tumors was determined using a γ counter (Perkin Elmer), with an energy window between 350 and 650 keV. We calculated the %ID per gram by normalizing the acquired counts to the injected dose of the respective tracer and the weight of the tumors.

Histologic and Immunohistologic Analysis

Tumor tissues were fixed in 3.7% formalin and processed for further histologic analysis as described before (*24*). Sections of 3 μm were stained with hematoxylin and eosin. Immunhistochemistry of paraffin-embedded sections was performed using the avidin biotin complex method as described previously with the following antibodies: Ki-67 (DAKO) and glucose transporter 1 (GLUT1; Thermo Fischer) (*24*).

Statistical Analysis

Statistical analysis was performed by 1-way ANOVA on ranks test and Student 2-tailed *t* test. All numeric data are expressed as mean ± SD. Significance was assumed for all *P* values of less than 0.05. Linear regression analysis was done using GraphPad Prism (GraphPad Software).

RESULTS

Establishment of Animal Model of Disseminated Rhabdomyosarcoma

Intraperitoneal injection of Rh30 cells resulted in tumor growth in 7 of 8 mice. Engraftment of RD cells was observed only in 4 of

TABLE 1
Experimental Design

Experiment	Transplanted cells	Tumor growth (n/n)	Monitoring
1	Rh30-mCherry-GLuc	3/4	OI, serum GLuc
	RD-mCherry-GLuc	2/5	
2	Rh30-mCherry-GLuc	4/4	OI, PET/MR imaging (^{18}F-FDG, ^{18}F-FLT), serum GLuc
	RD-mCherry-GLuc	2/4	
3	Rh30-mCherry-GLuc	9/10	OI, PET/MR imaging (^{18}F-FDG, ^{18}F-FLT, ^{11}C-choline), serum GLuc
4	Rh30-mCherry-GLuc	8/10	OI, biodistribution, serum GLuc
5	Rh30-mCherry-GLuc	8/9	Treatment with vincristine
			OI, PET/MR imaging (^{18}F-FDG, ^{18}F-FLT), biodistribution, serum GLuc

TABLE 2
Experimental Design for PET Scans

Tracer	Dose (MBq)	Uptake	Condition
^{18}F-FDG	12	1.0 h	Fasted 8–10 h before injection; anesthesia and heated during tracer uptake, 10-min static PET scan
^{18}F-FLT	12	1.5 h	Awake during tracer uptake, 10-min static PET scan
^{11}C-choline	4	10 min	Anesthesia during tracer uptake, 10-min static PET scan

9 mice (Table 1, experiments 1 and 2). The major differences between the different experiments were not discernable, and the total tumor take rate for Rh30 was 34 of 37. Thus, the RD mouse model was not explored further. Compared with baseline measurements, GLuc serum levels were increased in mice with Rh30-derived tumors 14 d after Rh30 injection and increased over the following week (Fig. 1A). The OI of the identical mice revealed mCherry fluorescence mainly in subcutaneous tumors located at the site of the cell injection (Fig. 1B). Abdominal exploration after animal sacrifice and subsequent postmortem OI with the skin removed revealed a large number of tumors. Only large subcutaneous tumors and a few of the smaller intraperitoneal tumors could be visualized with fluorescence imaging (Fig. 1B). Dissection and OI of the isolated organs revealed that tumors were present at the injection site and infiltrating abdominal muscles, liver, stomach, spleen, bladder, and different parts of the duodenum and colon (Fig. 2A). Rh30 tumor cell infiltration of the ovaries was also observed in the female mice.

At necropsy, a median of 37 Rh30 tumors (range, 27–50) were detected in 7 of 8 mice. The embryonal rhabdomyosarcoma cell line RD led to 26 tumors (range, 16–43) in 4 of 9 dissected mice (data not shown). The fluorescence intensities of the Rh30 tumors correlated with the respective area of the tumors; however, a large variance in the tumor size was observed (median, 2.9 mm^2; 0.14–47 mm^2) (Fig. 2B). Fluorescence signal areas of less than 1 mm^2 detected on OI at necropsy were reevaluated with fluorescence microscopy to confirm the Rh30 tumors. Histologic analysis of representative tumors revealed the characteristics of an alveolar rhabdomyosarcoma, which were composed of a dense cellular sheet of primitive rhabdomyoblasts (Supplemental Fig. 1). The Rh30 tumors showed infiltration into adjacent tissues, especially in the muscles, ovaries, and spleen. In contrast, tumor nodules in the liver and in the duodenum were encapsulated. Tumors were found to be highly proliferative based on Ki-67 immunhistochemistry (Supplemental Fig. 2). A high expression of the GLUT1 was observed heterogeneously and limited to distinct regions in the tumor nodules. Immunhistochemistry of GLUT1 revealed a higher expression in the tumors localized in the muscle than tumors that were disseminated in the liver. Evaluation of a published gene expression database of primary tissues (*27*) revealed a higher expression of glucose transporters, GLUT1 and GLUT3, in rhabdomyosarcoma than in muscle samples, but expression was at a low level (Supplemental Fig. 3). Enzymes involved in sequestering thymidine in cells, including thymidine kinase-1 and especially thymidine monophosphate kinase, were 2- and 4-fold, respectively, overexpressed in rhabdomyosarcoma in the same database. Therefore, tracers such as ^{18}F-FDG and ^{18}F-FLT may have the potential to reveal these tumors based on PET analysis.

Detection of Disseminated Rhabdomyosarcoma Tumors by PET/MR Imaging

Our experimental design (Table 1, experiments 2 and 3) includes the monitoring of tumor growth by OI and sequential PET/MR imaging using ^{18}F-FDG and ^{18}F-FLT tracers 3 wk after intraperitoneal xenotransplantation of Rh30 cells in NOD/LtSz-scid-IL2R$^{-/-}$ mice on the same experimental day. ^{11}C-choline PET was performed 2 d later.

PET/MR imaging confirmed the distinct growth patterns of Rh30 tumors as already shown by OI (Fig. 1B). On the basis of sequential PET/MR imaging with ^{18}F-FDG and ^{18}F-FLT tracers, rhabdomyosarcoma lesions were identified in vivo next to the stomach, spleen, and bladder as well as in different locations in the intestine and in the subcutaneous tissue at the injection site. Anatomic information from MR imaging is essential because the tumors did not show a homogeneous uptake of ^{18}F-FDG or ^{18}F-FLT (Figs. 3A and 3C). In addition, tiny lesions, which appear suspicious on MR imaging, could be clearly identified after coregistration with the respective ^{18}F-FDG or ^{18}F-FLT PET scan.

With ^{18}F-FLT as the PET tracer, the detection of very tiny lesions was achieved because of a high uptake by the rhabdomyosarcoma tumors and a low background signal in the peritoneal cavity (Figs. 3A and 3B). Approximately 5 rhabdomyosarcoma tumors were detected per animal, with a minimum tumor size of 1.2 mm in diameter. Although the ^{18}F-FLT injection yielded a strong tracer accumulation in the bladder, the detection of rhabdomyosarcoma tumors located near the bladder was possible (Fig. 3A). ^{18}F-FDG revealed an uptake in Rh30 tumors within the peritoneal cavity, intestine, and subcutaneous tumors. A strong nontumor tissue uptake of the tracer was observed in the kidneys,

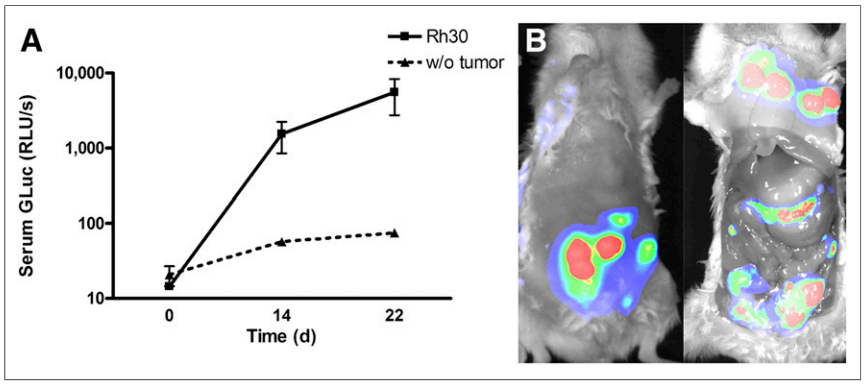

FIGURE 1. In vivo detection of Rh30 tumors by reporter gene expression. (A) Tumor growth was monitored by GLuc activity in serum (n = 9). GLuc activity was elevated and increased with observation time in mice with tumors (mean ± SD). Background activity of less than 100 relative light units per second (RLUs/s) was detected in mice without tumors (n = 5). (B) Rh30 tumors were detected by in vivo fluorescence OI for mCherry expression 3 wk after xenotransplantation (left). By necropsy, large subcutaneous and more intraperitoneal tumors were visualized by fluorescence OI (right). w/o = without.

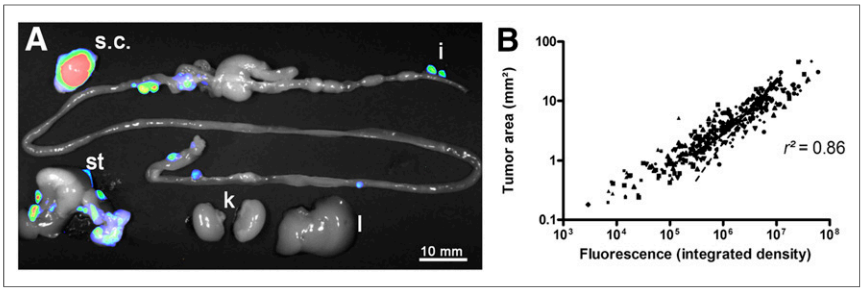

FIGURE 2. Ex vivo OI detection of Rh30 tumors. (A) Liver (l), stomach (st), kidneys (k), intestine (i), and skin (s.c.) were explanted 21 d after xenotransplantation of Rh30 cells. Tumor nodules were revealed by fluorescence OI. (B) Size of tumors from 10 mice correlates with fluorescence intensity at necropsy (331 tumors from 9 mice).

brown fat tissue, and intestine. Nevertheless, in combination with MR imaging, it was possible to accurately detect approximately 3.5 rhabdomyosarcoma tumors per animal, most of which were larger lesions that were clusters of tumors, with the smallest detected tumor size being 3 mm^3 (Figs. 3C and 3D). The analysis of ^{11}C-choline PET scans revealed no specific uptake of ^{11}C-choline in the peritoneal or subcutaneous rhabdomyosarcoma tumors (Supplemental Fig. 4).

The quantitative analysis of the PET scans revealed a slightly enhanced uptake of ^{18}F-FLT (3.5 ± 1.8 %ID/cm^3), compared with the uptake of ^{18}F-FDG (2.7 ± 0.3 %ID/cm^3) (Fig. 4A). The analysis of the tumor-to-muscle ratios (TMRs) showed a significant ($P < 0.05$) 2.5-fold-higher TMR for ^{18}F-FLT (5.0 ± 2.0) than for ^{18}F-FDG (2.0 ± 0.4) because of the low background signal of ^{18}F-FLT (Fig. 4A). At necropsy, tumors from 8 mice were detected on the basis of their mCherry fluorescence, and up to 19 nodules from different tissues per mouse were explanted to quantify the uptake of ^{18}F-FDG or ^{18}F-FLT by ex vivo γ counting (Table 1, experiment 4). A higher uptake and TRM were observed for ^{18}F-FLT than for ^{18}F-FDG ex vivo (Fig. 4B). The interrelation between tumor weight and the measurements on OI (area and fluorescence intensity) was explored. We detected a linear correlation between tumor weight and the fluorescence intensity in mice that underwent biodistribution investigations (r^2 = 0.41 for ^{18}F-FDG and 0.31 for ^{18}F-FLT) (Supplemental Figs. 5A and 5B). Outliners were reviewed by morphology and histology. Some samples with high weight and low fluorescence signal were confirmed as heterogeneous tissue with low tumor content. After these samples were excluded from the analysis, a better linear correlation was observed (r^2 = 0.85 for ^{18}F-FDG and 0.86 for ^{18}F-FLT, data not shown). The analysis of the biodistribution data also revealed a linear correlation between incorporated tracer activity and fluorescence intensity (r^2 = 0.80 for ^{18}F-FLT and 0.42 for ^{18}F-FDG (Supplemental Figs. 5C and 5D).

Detection of Tumors During Chemotherapy

The detection and localization by imaging modalities of Rh30 tumors are essential for surgical treatment. In clinical practice at this stage of therapy, various courses of chemotherapeutic drugs that might alter tumor metabolic activity have been applied. Thus, we evaluated the feasibility of PET/MR imaging to detect rhabdomyosarcoma after chemotherapy with vincristine (Table 1, experiment 5). In 8 of 9 mice, tumor engraftment was detected 21 d after injection of Rh30 cells based on the measurement of GLuc activity in the serum, OI, and PET/MR imaging with ^{18}F-FDG and ^{18}F-FLT tracers before the initiation of treatment. Mice were administered vincristine over 2 consecutive days after the ^{18}F-FLT/^{18}F-FDG PET/MR imaging baseline measurement, and monitoring of tumor growth was repeated 2 and 4 wk later by PET/MR imaging.

Baseline PET/MR imaging showed a slightly higher %ID/cm^3 of ^{18}F-FLT in intraperitoneal rhabdomyosarcoma tumors than ^{18}F-FDG. However, 2 wk after treatment with vincristine, the ^{18}F-FLT uptake was reduced by a factor of 2.8 (P = 0.002, Student t test; baseline, 3.64 ± 0.9 %ID/cm^3; 2 wk after treatment, 1.32 ± 0.52 %ID/cm^3), whereas ^{18}F-FDG uptake remained at constant levels, compared with the baseline measurement (baseline, 2.96 ± 0.25 %ID/cm^3; 2 wk after treatment, 3.51 ± 0.40 %ID/cm^3; Figs. 5A and 5B). Treatment with vincristine clearly inhibited the tumor cell proliferation but displayed hardly any impact on the glucose consumption in the rhabdomyosarcoma tumors. PET/MR imaging in week 4 after vincristine treatment yielded a recovery of the proliferation and thus an enhanced ^{18}F-FLT uptake, compared with the previous measurement at week 2 (1.91 ± 0.81 %ID/cm^3). However, several animals displayed a decreased ^{18}F-FLT uptake, indicating a maintained therapy response to vincristine. Tumor volumetry with MR imaging of 4 representative animals indicated a slight increase in the tumor volume 2 wk after vincristine treatment, compared with the baseline measurement. Four weeks after vincristine treatment, the tumor volume

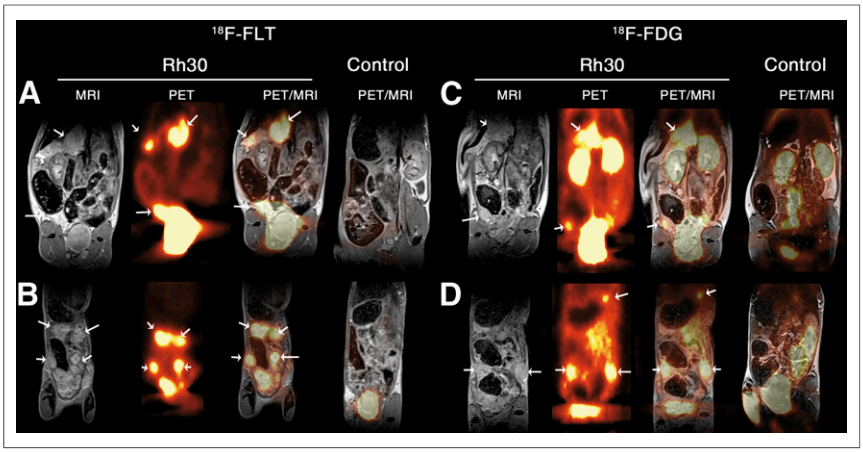

FIGURE 3. In vivo detection of Rh30 tumors by sequential PET/MR imaging. Rh30 tumors were detected by ^{18}F-FLT PET/MR imaging in the intraperitoneal cavity (A) and with focus on subcutaneous/intraperitoneal tumors with high contrast, due to low background signal in the peritoneal cavity (B). ^{18}F-FDG PET/MR imaging with the same mice detected identical tumors (C and D) but with lower sensitivity than ^{18}F-FLT due to ^{18}F-FDG signals in kidneys, bladder, and intestine. For comparison, fused PET/MR images of control mice without tumors (control) are shown. Tumors are indicated by arrows.

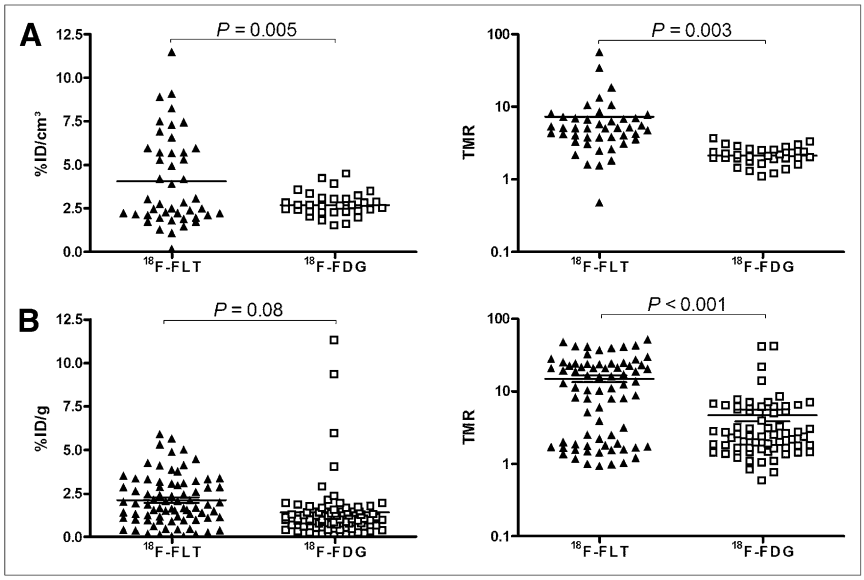

FIGURE 4. Comparison of ^{18}F-FLT and ^{18}F-FDG tracers for detection of Rh30 tumors. Tumors were detected in 9 mice using PET/MR imaging. In these mice, 44 tumors were detected using ^{18}F-FLT and 36 using ^{18}F-FDG. (A) Uptake of tracer for each tumor is expressed as %ID/cm^3 and TMR. Tracer uptake and TMR were significant higher for ^{18}F-FLT than for ^{18}F-FDG (Student *t* test). (B) Rh30 tumors were evaluated at necropsy to analyze uptake of ^{18}F-FDG ($n = 4$) and ^{18}F-FLT ($n = 4$) by ex vivo γ counting.

was reduced in 4 representative animals ($P = 0.04$, Student *t* test) (Fig. 5C). A linear correlation between tumor volume as detected by MR imaging and the GLuc activity in serum was observed ($r^2 = 0.85$, Fig. 5C). The tumors after vincristine treatment were characterized by anaplastic cells. In this representative example, the tumors showed lower density of Ki-67 and an expression pattern of GLUT1 that was similar to the controls (Supplemental Figs. 2D–2F).

DISCUSSION

We successfully established a new animal model of disseminated alveolar rhabdomyosarcoma enabling us to address complex questions regarding tumor biology, immunology, imaging, and development of novel treatment approaches in an orthotopic setting in further studies.

Orthotopic human rhabdomyosarcoma were developed using alveolar Rh30 and embryonal RD cells. The efficient growth of Rh30, compared with the RD tumors, may be a result of the different genetic backgrounds of the tumor entities, for which alveolar rhabdomyosarcomas (Rh30) are aggressive and show nodal and distant metastatic growth and local invasiveness. The stable transfection of cells with reporter genes coding for fluorescent proteins (mCherry) and luciferase (GLuc) facilitate in vivo OI and the detection of serum levels of reporter enzymes, respectively. Diffuse bioluminescence signals were observed in the abdomen in the first 5 min after intraperitoneal injection of the GLuc substrate coelenterazine; however, the location of the bioluminescence signals did not overlap with the tumor position (data not shown). This may be a result of the diffuse distribution of the secreted luciferase in the peritoneal cavity and the inhomogeneous distribution of the fast-precipitating coelenterazine (*28*). Our model of disseminated rhabdomyosarcoma can be adopted for drug screening using reporter enzyme activity in the serum. In the disseminated model of Rh30 tumors, a decrease in tumor burden was revealed by GLuc activity in the serum and tumor volume (PET/MR imaging), demonstrating the efficiency of vincristine.

In this study, we used the model for the preclinical evaluation of sequential PET/MR imaging. The combined molecular and morphologic information as provided by PET/MR imaging is considered to be powerful for the detection of rhabdomyosarcoma recurrence, for which scar formation impairs an accurate assessment based on the information from a single imaging modality or PET/CT, which is limited by the weak soft-tissue contrast of the CT. ^{18}F-FDG PET/CT sensitivity was found to be superior to that of conventional imaging modalities, consisting of MR imaging of the primary site, whole-body CT, and bone scintigraphy, for the determination of lymph node involvement and the detection of metastases (*7*). However, one major drawback of the application of PET/CT in the detection of rhabdomyosarcoma in children is the high effective radiation dose of typically 10 mSv after the required chest, abdomen, and pelvis CT scans. PET studies for the detection of rhabdomyosarcoma were performed at a body weight–adapted activity of 4 MBq of ^{18}F-FDG/kg of body weight (*5*).

In the presented mouse model, a comparison of ^{18}F-FLT and ^{18}F-FDG tracers for the detection and therapy monitoring of disseminated rhabdomyosarcoma was performed by sequential PET/MR imaging. Because of the low background signal in the peritoneal cavity, ^{18}F-FLT PET/MR imaging proved to be superior to ^{18}F-FDG PET/MR imaging. The combination of PET and MR imaging enables a clear identification of small rhabdomyosarcoma lesions (diameter, 1.2 mm) in vivo. In mice, the detection of rhabdomyosarcoma tumors smaller than 0.9 mm was only possible in the reciprocal analysis of fused PET and MR images. The Rh30 tumors detected by PET/MR imaging were larger than those observed by OI at necropsy, which may be a result of trabecular growth of tumors in few regions. Those regions were assessed in PET/MR imaging as singular tumors, and therefore a smaller number of tumors were detected with PET/MR than with fluorescence imaging at necropsy. The improved detection sensitivity of ^{18}F-FLT, compared with ^{18}F-FDG, can also be expected in humans, as the expression of glucose transporters was 2-fold higher and that of thymidine monophosphate kinase was 4-fold higher in rhabdomyosarcoma than in muscle tissue (*27*). With the recently introduced clinical PET/MR imaging scanner, simultaneous data acquisition is feasible with a short scan time and low radiation dose, which is specifically important in pediatrics. Thus, our study has a high potential for clinical translation.

Other tracers for PET such as ^{18}F-fluoromethylcholine were tested in a model of rat subcutaneous rhabdomyosarcoma to monitor radiation therapy (*17*). This study could be not reproduced in our model by applying ^{11}C-choline as a PET tracer, where human-derived rhabdomyosarcoma grew intraperitoneally. The tracer did not accumulate in human-derived Rh30 rhabdomyosarcoma, and the background, especially in the liver and kidneys, was high. Still, choline may be considered as a valuable tracer in humans, because preliminary results of a ^{11}C-choline PET/CT study showed improved accuracy of staging in patients with bone and soft-tissue sarcomas, among them one of whom had rhabdomyosarcoma, compared with conventional imaging (*29*).

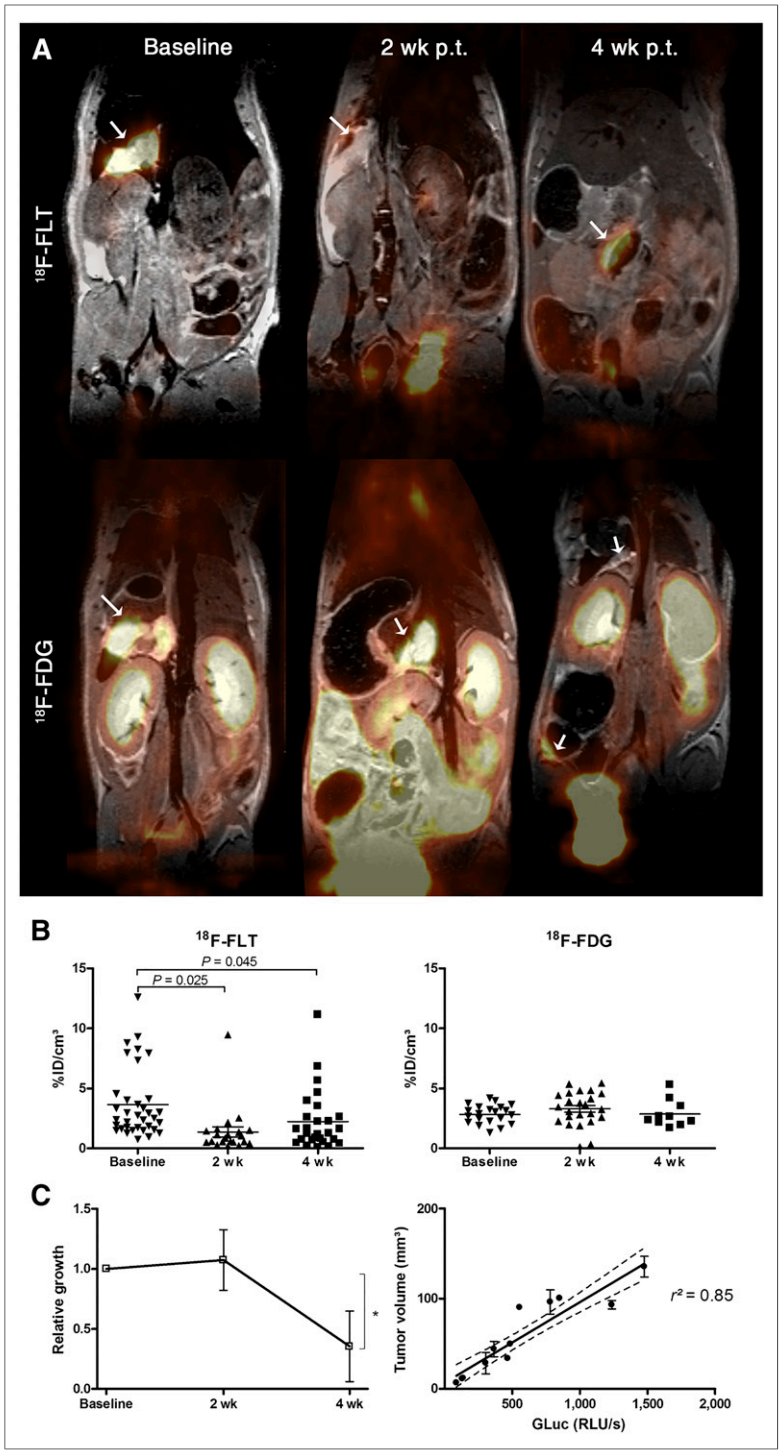

FIGURE 5. Therapy monitoring of Rh30 tumors by sequential PET/MR imaging. Rh30 tumors were detected by PET/MR imaging using tracers ^{18}F-FLT or ^{18}F-FDG before (baseline) and at 2 and 4 wk after vincristine injection. (A) Merged PET/MR images of identical representative mice after ^{18}F-FLT and ^{18}F-FDG uptake at every investigated time point are shown. Tumors are indicated by arrows. (B) Analysis of ^{18}F-FLT or ^{18}F-FDG uptake is expressed as %ID/cm^3 for each detected tumor at distinct time point. Analysis revealed reduced ^{18}F-FLT uptake in rhabdomyosarcoma tumors 2 wk after vincristine injection, whereas ^{18}F-FDG uptake remained constant after vincristine treatment. (C) Total tumor volume of 4 experimental mice as determined by MR imaging and ^{18}F-FLT/^{18}F-FDG PET was related to baseline measurement before treatment and revealed significant decrease of tumor burden 4 wk after treatment with vincristine (*P = 0.04, Student t test). Summated tumor volumes are linear proportional to serum GLuc activity. RLU/s = relative light units per second.

PET imaging has the potential to be predictive of an early and long-term response to cancer therapy. In our study, ^{18}F-FLT showed an initial response of disseminated rhabdomyosarcoma to cytotoxic drugs such as vincristine after 2 wk, but this response disappeared 4 wk after treatment. A similar transient response to kinase inhibitors could be successfully monitored using ^{18}F-FDG in small-animal PET imaging in mice rhabdomyosarcoma in a genetically engineered model (*20*). In contrast, ^{18}F-FDG uptake in human rhabdomyosarcoma remained constant after vincristine treatment. Considering the significantly smaller tumor lesions after therapy and the potential partial-volume effect influencing imaging quantification in smaller lesions, the real %ID/cm^3 at 4 wk after treatment might most likely even be higher, as shown by Mannheim et al., comparing the quantification and recovery of different sphere sizes using the Inveon microPET. In spheres of 3.95-mm diameter, a 39.5% recovery in an 8:1 activity-to-background ratio was found (*30*), emphasizing a higher metabolic activity of the tumor cells after vincristine treatment.

The serum marker GLuc decreased during the treatment period and was correlated with the decreasing signal on the PET/MR imaging measurements, which was also reflected by the changed biology of the tumor cells during vincristine treatment as indicated by transition from a rhabdoid to a predominantly anaplastic morphology. This finding is expected from the known effects of vincristine, which binds to tubulin dimers, inhibiting assembly of microtubule structures and arresting mitosis in metaphase. The observed heterogeneous expression pattern of the glucose transporters in Rh30 tumors did not change during the treatment. Therefore, ^{18}F-FDG PET/MR imaging may be useful for detecting tumors; however, with ^{18}F-FLT PET/MR imaging is more likely to detect an initial drug response in rhabdomyosarcoma. A similar observation was made during chemoradiation of head and neck squamous cell carcinoma, for which ^{18}F-FLT PET signal change preceded ^{18}F-FDG PET change during therapy (*31*). ^{18}F-FLT PET seems promising for the early evaluation of chemoradiation effects as in tailoring therapy for rhabdomyosarcoma patients through early identification of responders and nonresponders similar to clinical experience in ovarian cancer (*32*). At present, in pediatric patients ^{18}F-FDG PET was superior to conventional imaging for response assessment in Hodgkin lymphoma (*33*). For detecting metabolically active rhabdomyosarcoma during treatment, ^{18}F-FDG seemed to be more sensitive; however, ^{18}F-FLT with a higher TMR could be a better choice for identifying rhabdomyosarcoma at the initial diagnosis.

CONCLUSION

With the presented model for disseminated rhabdomyosarcoma, we showed the potential of PET/MR imaging to detect small rhabdomyosarcoma tumors

based on molecular and anatomic information. Thus, PET/MR imaging could help detect disseminated small tumors, with the improved differentiation between tumors and scars in advanced and recurrent tumors, and therefore the modality might influence therapeutic decisions in the future.

DISCLOSURE

The costs of publication of this article were defrayed in part by the payment of page charges. Therefore, and solely to indicate this fact, this article is hereby marked "advertisement" in accordance with 18 USC section 1734. Bernd J. Pichler is a consultant for Siemens Medical Solutions. No other potential conflict of interest relevant to this article was reported.

ACKNOWLEDGMENTS

We thank Julia Wenz, Bettina Kirchner, and Funda Cay for excellent technical support.

REFERENCES

1. Crist W, Gehan EA, Ragab AH, et al. The Third Intergroup Rhabdomyosarcoma Study. *J Clin Oncol.* 1995;13:610–630.
2. Maurer HM, Gehan EA, Beltangady M, et al. The Intergroup Rhabdomyosarcoma Study-II. *Cancer.* 1993;71:1904–1922.
3. National Cancer Institute. *Childhood Rhabdomyosarcoma Treatment*. Cancer.gov. November 26, 2013. http://cancer.gov/cancertopics/pdq/treatment/childrhabdomyosarcoma/HealthProfessional. Accessed June 9, 2014.
4. Völker T, Denecke T, Steffen I, et al. Positron emission tomography for staging of pediatric sarcoma patients: results of a prospective multicenter trial. *J Clin Oncol.* 2007;25:5435–5441.
5. Baum SH, Fruhwald M, Rahbar K, Wessling J, Schober O, Weckesser M. Contribution of PET/CT to prediction of outcome in children and young adults with rhabdomyosarcoma. *J Nucl Med.* 2011;52:1535–1540.
6. Mody RJ, Bui C, Hutchinson RJ, et al. FDG PET imaging of childhood sarcomas. *Pediatr Blood Cancer.* 2010;54:222–227.
7. Eugene T, Corradini N, Carlier T, Dupas B, Leux C, Bodet-Milin C. ^{18}F-FDG-PET/CT in initial staging and assessment of early response to chemotherapy of pediatric rhabdomyosarcomas. *Nucl Med Commun.* 2012;33:1089–1095.
8. Chawla SC, Federman N, Zhang D, et al. Estimated cumulative radiation dose from PET/CT in children with malignancies: a 5-year retrospective review. *Pediatr Radiol.* 2010;40:681–686.
9. Kumar R, Shandal V, Shamim SA, Halanaik D, Malhotra A. Clinical applications of PET and PET/CT in pediatric malignancies. *Expert Rev Anticancer Ther.* 2010;10:755–768.
10. Bailey DL, Barthel H, Beyer T, et al. Summary report of the First International Workshop on PET/MR imaging, March 19–23, 2012, Tubingen, Germany. *Mol Imaging Biol.* 2013;15:361–371.
11. Judenhofer MS, Wehrl HF, Newport DF, et al. Simultaneous PET-MRI: a new approach for functional and morphological imaging. *Nat Med.* 2008;14:459–465.
12. Sauter AW, Wehrl HF, Kolb A, Judenhofer MS, Pichler BJ. Combined PET/MRI: one step further in multimodality imaging. *Trends Mol Med.* 2010;16:508–515.
13. Schmid A, Schmitz J, Mannheim JG, et al. Feasibility of sequential PET/MRI using a state-of-the-art small animal PET and a 1 T benchtop MRI. *Mol Imaging Biol.* 2013;15:155–165.
14. Pichler BJ, Kolb A, Nagele T, Schlemmer HP. PET/MRI: paving the way for the next generation of clinical multimodality imaging applications. *J Nucl Med.* 2010;51:333–336.
15. Wehrl HF, Schwab J, Hasenbach K, et al. Multimodal elucidation of choline metabolism in a murine glioma model using magnetic resonance spectroscopy and ^{11}C-choline positron emission tomography. *Cancer Res.* 2013;73:1470–1480.
16. Dubois L, Landuyt W, Cloetens L, et al. [^{18}F]EF3 is not superior to [^{18}F]FMISO for PET-based hypoxia evaluation as measured in a rat rhabdomyosarcoma tumour model. *Eur J Nucl Med Mol Imaging.* 2009;36:209–218.
17. Rommel D, Abarca-Quinones J, Bol A, et al. Early monitoring of external radiation therapy by [^{18}F]-fluoromethylcholine positron emission tomography and 3-T proton magnetic resonance spectroscopy: an experimental study in a rodent rhabdomyosarcoma model. *Nucl Med Biol.* 2010;37:645–653.
18. Rommel D, Abarca-Quinones J, Christian N, et al. Alginate moulding: an empirical method for magnetic resonance imaging/positron emission tomography co-registration in a tumor rat model. *Nucl Med Biol.* 2008;35:571–577.
19. Rommel D, Bol A, Abarca-Quinones J, et al. Rodent rhabdomyosarcoma: comparison between total choline concentration at H-MRS and [^{18}F]-fluoromethylcholine uptake at PET using accurate methods for collecting data. *Mol Imaging Biol.* 2010;12:415–423.
20. Soundararajan A, Abraham J, Nelon LD, et al. ^{18}F-FDG microPET imaging detects early transient response to an IGF1R inhibitor in genetically engineered rhabdomyosarcoma models. *Pediatr Blood Cancer.* 2012;59:485–492.
21. Benz MR, Czernin J, Allen-Auerbach MS, et al. 3′-deoxy-3′-[^{18}F]fluorothymidine positron emission tomography for response assessment in soft tissue sarcoma: a pilot study to correlate imaging findings with tissue thymidine kinase 1 and Ki-67 activity and histopathologic response. *Cancer.* 2012;118:3135–3144.
22. Cobben DC, Elsinga PH, Suurmeijer AJ, et al. Detection and grading of soft tissue sarcomas of the extremities with ^{18}F-3′-fluoro-3′-deoxy-L-thymidine. *Clin Cancer Res.* 2004;10:1685–1690.
23. Seitz G, Armeanu-Ebinger S, Warmann S, Fuchs J. Animal models of extracranial pediatric solid tumors. *Oncol Lett.* 2012;4:859–864.
24. Seitz G, Pfeiffer M, Fuchs J, et al. Establishment of a rhabdomyosarcoma xenograft model in human-adapted mice. *Oncol Rep.* 2010;24:1067–1072.
25. Keller C, Capecchi MR. New genetic tactics to model alveolar rhabdomyosarcoma in the mouse. *Cancer Res.* 2005;65:7530–7532.
26. Lieber J, Eicher C, Wenz J, et al. The BH3 mimetic ABT-737 increases treatment efficiency of paclitaxel against hepatoblastoma. *BMC Cancer.* 2011;11:362.
27. Herrmann D, Seitz G, Warmann SW, Bonin M, Fuchs JR, Armeanu-Ebinger S. Cetuximab promotes immunotoxicity against rhabdomyosarcoma in vitro. *J Immunother.* 2010;33:279–286.
28. Wurdinger T, Badr C, Pike L, et al. A secreted luciferase for ex vivo monitoring of in vivo processes. *Nat Methods.* 2008;5:171–173.
29. Tateishi U, Yamaguchi U, Maeda T, et al. Staging performance of carbon-11 choline positron emission tomography/computed tomography in patients with bone and soft tissue sarcoma: comparison with conventional imaging. *Cancer Sci.* 2006;97:1125–1128.
30. Mannheim JG, Judenhofer MS, Schmid A, et al. Quantification accuracy and partial volume effect in dependence of the attenuation correction of a state-of-the-art small animal PET scanner. *Phys Med Biol.* 2012;57:3981–3993.
31. Hoshikawa H, Mori T, Kishino T, et al. Changes in ^{18}F-fluorothymidine and ^{18}F-fluorodeoxyglucose positron emission tomography imaging in patients with head and neck cancer treated with chemoradiotherapy. *Ann Nucl Med.* 2013;27:363–370.
32. Tsuyoshi H, Morishita F, Orisaka M, Okazawa H, Yoshida Y. ^{18}F-fluorothymidine PET is a potential predictive imaging biomarker of the response to gemcitabine-based chemotherapeutic treatment for recurrent ovarian cancer: preliminary results in three patients. *Clin Nucl Med.* 2013;38:560–563.
33. Furth C, Steffen IG, Amthauer H, et al. Early and late therapy response assessment with [^{18}F]fluorodeoxyglucose positron emission tomography in pediatric Hodgkin's lymphoma: analysis of a prospective multicenter trial. *J Clin Oncol.* 2009;27:4385–4391.